Consideration of Formation Buffering Potential and Reactive Mineral Availability Pertaining to Geological Storage of Carbon Dioxide

B. R. Ellis, K. M. Bowman, C. A. Peters*, M. Buschkuehle†

Department of Civil and Environmental Engineering, Princeton University

***Corresponding author: cap@princeton.edu**
†Alberta Geological Survey, Edmonton, Canada

Abstract

One promising strategy for decreasing CO_2 emissions to the atmosphere is carbon capture and storage in deep saline formations. Modeling efforts and the experimental measurements that support these efforts are critical to determining the fate of injected CO_2. The focus of this work is CO_2-water-rock interactions as they pertain to formation buffering potential and reactive mineral availability. In addressing formation buffering potential, PHREEQC was used to model pH evolution in siliciclastic and carbonate rocks. The aim of this modeling is to evaluate host formation mineralogy based on the ability to buffer the acid created by CO_2 injection.

Our second goal is to better define mineral abundance and availability in siliciclastic sedimentary rocks, to support the development of relationships for upscaling reactive transport. Energy dispersive X-ray spectroscopy and backscattered electron microscopy were used to identify minerals and characterize the spatial distributions of potentially reactive minerals in thin sections from the Alberta Basin.

Modeling Formation Buffering Potential

The goal of this modeling effort was to compare the buffering potential of siliciclastic formations to that of carbonate formations. We are also interested in the extent of variability in buffering potential across formations of similar composition. In order to assess the buffering potential of various formations in the Alberta Basin, PHREEQC was used to determine pH conditions of the formation over 100 years with injected CO_2 at a pressure of 100 bar. Geochemical simulations were run at 50°C and 100 bar, representing typical injection conditions for a depth of 1 km. Six core samples and their accompanying formation water were collected and analyzed by the Alberta Geological Survey. Percent mineral composition for each sample is presented in the table below along with the corresponding formation water ionic strength and pH after 100 years. Each sample was assumed to have a porosity of 20% and a total rock mass of 12 kg.

Sample #	Formation Water Ionic Strength (m)	Initial Mineral Composition (%)	pH After 100 Years
MB14 Sandstone	3.9	Quartz(72), Dolomite(19.2), K-feldspar(4.3), Anorthite(1.4), Albite(1.4), Hematite(0.7), Anhydrite(0.5), Apatite(0.5)	4.40
MB01 Sandstone	4.5	Quartz(95.6), Kaolinite(1.8), Anhydrite(1.6), Calcite(0.4), K-feldspar(0.2), Pyrite(0.1), Magnesite(0.1)	4.17
MB04 Quartz Wacke	4.5	Kaolinite(39.0), Quartz(31.9), Muscovite(12.2), Illite(7.1), Albite(3.8), Anatase(1.9), K-feldspar(1), Pyrite(1.4), Dolomite(0.6), Magnesite(0.6), Siderite(0.3), Apatite(0.2)	4.47
MB07 Carbonate	1.02	Dolomite(82.9), Magnesite(9.7), Apatite(3.4), Quartz(2.9), Illite(0.8), Pyrite(0.2)	5.33
MB11 Carbonate	1.02	Dolomite(88.6), Magnesite(9.8), Apatite(0.8), Quartz(0.7), Hematite(0.1)	5.37
MB02 Carbonate	1.7	Calcite(78), Quartz(18.3),Apatite(1.5), Dolomite(1.1), K-feldspar(0.5), Pyrite(0.3), Albite(0.1), Kaolinite(0.1), Hematite(0.1)	4.61

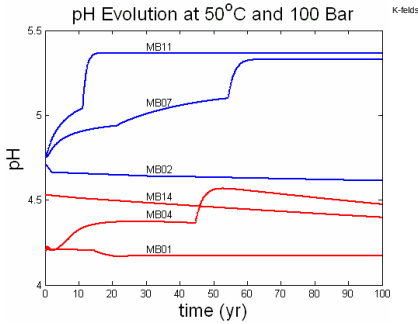

Carbonate formations will buffer the acidic brine to a higher pH than siliciclastic formations. There is also considerable variability of pH buffering within each type of formation.

Examples of acid-catalyzed mineral dissolution reactions resulting in pH buffering:

$$MgCO_3 + H^+ \leftrightarrow Mg^{2+} + HCO_3^-$$
Magnesite

$$2KAlSi_3O_8 + 2H^+ + 9H_2O \leftrightarrow Al_2Si_2O_5(OH)_4 + 2K^+ + 4H_4SiO_4$$
K-feldspar Kaolinite

MB04: change in mineral quantities during the 100 year geochemical simulation:

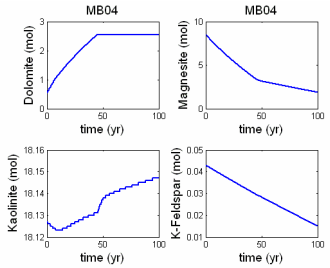

Surface Area Sensitivity Analysis

The reactive surface area of a mineral is usually assumed to be proportional to its abundance, but images captured by scanning electron microscopy show that mineral surfaces are often obscured by clay coatings. To examine the impact of mineral surface area overestimation, two simulations were run for the same sample: one assuming equal surface area per gram mineral and the other assuming kaolinite comprised 80% of the total surface area. The graph to the right illustrates that when kaolinite is the predominant mineral in contact with the pore fluids, the buffering reaction kinetics are retarded.

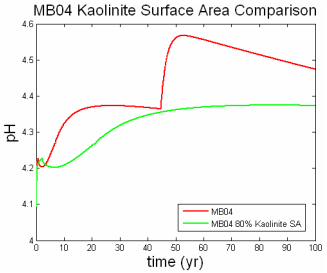

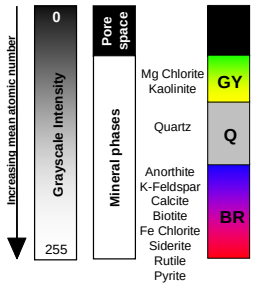

Prior Work: The backscattered electron (BSE) detector of the scanning electron microscope (SEM) was used to examine the spatial distribution of minerals in thin sections of sandstone samples from the Alberta Basin. Grayscale images are created using the BSE detector such that the intensity of a pixel is related to the mean atomic number of the material at that location. Using the processing scheme shown to the left, maps were created that identify pore space, quartz, minerals with mean atomic number less than quartz, and minerals with mean atomic number greater than quartz. The relative amount of each mineral category was calculated, as well as the amount adjacent to pore space.

Reactive Mineral Availability

Prior BSE Image Processing Results: The minerals that are most important in pH buffering tend to have a mean atomic number greater than quartz. Processing 90 BSE images from three different sandstones showed that the availability of these minerals to the pore space is only 20% of their abundance. However, BSE images do not provide enough information to make these calculations for individual minerals.

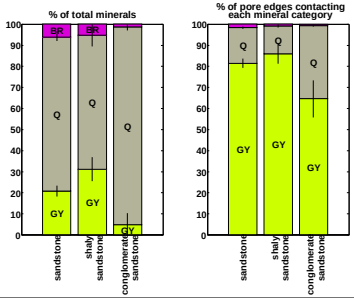

The goal of this work was to develop a methodology for quantifying the available surface area of individual minerals. We developed a procedure by which energy dispersive X-ray (EDX) spectroscopy is used to locate specific elements and identify minerals by combining the element maps. The EDX cannot provide adequate information about aluminum, however, so some minerals (e.g. quartz and kaolinite) cannot be distinguished.

We have developed an algorithm for combining EDX maps with BSE maps, which do distinguish quartz from kaolinite. Once the minerals have been identified, the amount of each mineral present and adjacent to the pore space is calculated.

Example of combined EDX and BSE analysis:

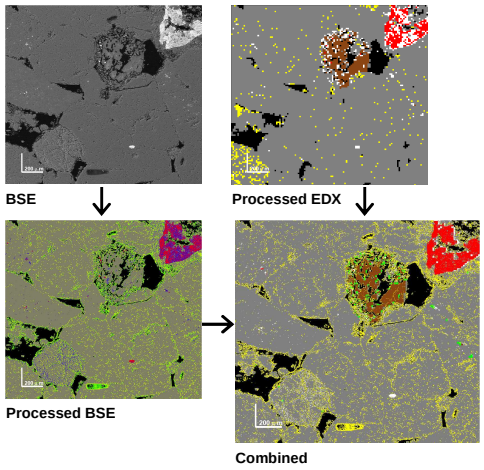

In this image, 9% of the mineral matter is kaolinite, but it coats 80% of the pore perimeter, obscuring reactive minerals.

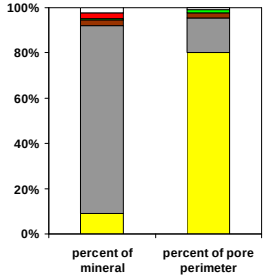

	percent of image	percent of mineral	percent of pore perimeter
pore space	8.10	n/a	n/a
kaolinite	8.48	9.22	80.21
quartz	76.15	82.86	15.21
apatite	2.20	2.40	2.39
plagioclase	0.53	0.57	1.20
pyrite	2.34	2.55	0.21
unidentified	2.20	2.39	0.78

Conclusions

The modeling results demonstrate that there is high variability of kinetic reactions, even within formations of similar mineral composition. As expected, the carbonate formations buffered the acidic solution much faster than the siliciclastic formations. However, the full buffering capacity of the siliciclastic formations was not exhausted during the 100 year simulation.

Future modeling work will include further investigation of the buffering potential of different formations over longer periods of time. Ultimately, the motivation of this work is to provide yet another tool for determining optimal CO_2 injection aquifers.

The EDX/BSE image analysis method shows great potential for determining reactive mineral availability and better surface area estimations. Incorporation of these results into reactive transport models will allow for more accurate representation of formation reactivity with injected CO_2.

Future imaging work will focus on analyzing additional samples and characterizing a statistical relationship between the abundance of reactive minerals and their available surface area.

The authors acknowledge the financial support by Department of Energy, Office of Basic Energy Sciences, through Grant No. DE-FG02-05ER15636.